Biomaterials 272 (2021) 120757

Contents lists available at ScienceDirect

Biomaterials

journal homepage: www.elsevier.com/locate/biomaterials

Targeted regulation of lymphocytic ER stress response with an overall immunosuppression to alleviate allograft rejection

Yingying Shi, Yichao Lu, Chunqi Zhu, Zhenyu Luo, Xiang Li, Yu Liu, Mengshi Jiang, Xu Liu, Lihua Luo, Yongzhong Du, Jian You *

College of Pharmaceutical Sciences, Zhejiang University, 866 Yuhangtang Road, Hangzhou, Zhejiang, 310058, PR China

ARTICLE INFO

Keywords:
Allograft rejection
Lymphocyte
IRE1α
ER-targeting
$CD8^+$ T cells
Immunosuppression

ABSTRACT

Transplantation is the most effective, and sometimes the only resort for end-stage organ failure. However, allogeneic graft suffers greatly from lymphocyte-mediated immunorejection, which bears close relationship with a hyperactivation of endoplasmic reticulum (ER) stress response in host lymphocytes, especially in $CD8^+$ T cells (T-8). Therefore, regulating lymphocytic ER unfolded protein response (UPR) might be a potential therapeutic breakthrough in alleviating graft rejection. Here, ER-targetable liposome is prepared via the surface modification of ER-targeting peptide (Pardaxin), which efficiently loads and directly delivers small molecule inhibitor of UPR sensor IRE1α into the ER of lymphocytes, inducing a systemic immunosuppression that facilitates tumorigenesis and metastasis in the tumor inoculation challenge *in vivo*. And *in vitro*, a stage-differential dependency of IRE1α in the phase transition of T-8 is identified. Specifically, inhibiting IRE1α at the early responding stages of T-8, especially at the activation phase, results in a shrunk proliferation, impaired effector function, and limited memory commitment, which might contribute centrally to the induced overall immunosuppression. Based on this, a classical acute rejection model, murine full-thickness trunk skin allograft that primary arises from the hyperactivity of T-lymphocyte, is used. Results suggest that lymphocytic IRE1α inactivation attenuates transplant rejection and prolongs graft survival, with a limited effector function and memory commitment of host T-8. Moreover, an even higher immunosuppressive effect is obtained when IRE1α inhibition is used in combination with immunosuppressant tacrolimus (FK506), which might owe to a synergistic regulation of inflammatory transcription factors. These findings provide a deeper insight into the biological polarization and stress response of lymphocytes, which might guide the future development of allogeneic transplantation.

1. Introduction

Organ transplantation is the medical procedure where an allogeneic or autogenous organ from donor is used to replace a damaged or missing one in recipient. It is the most effective, and sometimes the only available resort for end-stage organ failure [1,2]. When the accessibility of autografts is limited, which is frequently faced in clinical practice, allogeneic transplantation become an alternative. However, allograft suffers greatly from an unavoidable host versus graft rejection, which seriously impairs the survival of transplanted organs and lowers the living quality of recipients. Emerging evidence suggests that allograft rejection is largely mediated by lymphocytes, especially $CD8^+$ T cells (T-8) [3–5]. It's demonstrated that the massive clonal expansion and cytotoxic attacking of effector T-8 accounts primarily for the acute cellular rejection (ACR) that occurs early post graft [6], whereas the persistence of memory T-8 imposes great risks of chronic rejection in the long run [7–9]. Generally, patient that receives allogeneic organ is asked to take immunosuppressive drugs (IS) indefinitely, so as to inhibit the overall immunity, prolong postoperative rejection, and improve the survival of grafted organs. Clinically used IS mainly include monoclonal-/polyclonal-antibodies, calcineurin inhibitor (CaNI), anti-proliferation drugs, glucocorticoids and mammalian target of rapamycin inhibitor (mTORi). However, lacking specificity and selectivity over target cells, most IS are ineffective and even invalid in mitigating acute rejection, and a long-term administration might impair the systematic immunity and even bear risks of inducing severe complications, such as bone marrow suppression, opportunistic infection, metabolic syndrome and kidney damage [10,11]. Therefore, a new immunosuppressive strategy with high efficiency and low toxicity is in urgent need.

* Corresponding author. College of Pharmaceutical Sciences, Zhejiang University, 866 Yuhangtang Road, Hangzhou, 310058, Zhejiang, PR China.
E-mail address: youjiandoc@zju.edu.cn (J. You).

https://doi.org/10.1016/j.biomaterials.2021.120757
Received 5 November 2020; Received in revised form 5 March 2021; Accepted 12 March 2021
Available online 24 March 2021

Unfolded protein response (UPR) is one of the most conserved adaptive mechanisms that facilitates the proteostasis remodeling of endoplasmic reticulum (ER). Environmental insult, nutrient fluctuation, or activation stimulus induces an excessive accumulation of malfolded proteins in the ER lumen, causing ER stress, and thus initiating UPR. In eukaryotes, UPR signaling is independently sensed and mediated by three ER-transmembrane transducers: inositol-requiring enzyme 1α (IRE1α, also known as ERN1), protein kinase R-like ER kinase (PERK, also known as EIF2AK3), and activating transcription factor 6 (ATF6). As the most conserved UPR branch, IRE1α axis alleviates ER burden mainly by elevating the protein processing capacity of cells, which is ubiquitously involved in the biological activities of multiple immune cells [12–14], including the development and activation response of T-/B- lymphocytes [15–18], the antigen presentation of dendritic cells [19], the polarization of macrophages [20], and the effector functioning of NK cells [13], displaying regulatory potential in reshaping systemic immunity.

It's observed that lymphocyte-mediated allogeneic graft rejection is usually accompanied by a hyperactivation of lymphocytic ER stress response. However, it's still poorly understood what role UPR, IRE1α in particular, plays in lymphocyte-associated transplant rejection. We hypothesize that regulating lymphocytic UPR might be a potential therapeutic breakthrough in allogeneic transplantation. Here, ER-targetable liposome features easy preparation, flexible drug loading, and excellent cellular uptake is constructed to efficiently deliver small molecule inhibitors of UPR sensors into the ER of lymphocytes, so as to induce an overall immunosuppression for a better skin allograft outcome, which bears close correlation with the stage-differential dependency of UPR by T-8. Our results help to gain a deeper insight into the biological polarization and stress response of lymphocytes in transplantation rejection, which may guide the future treatment of hyperimmunity-derived diseases and disorders, such as graft rejection, inflammatory diseases, autoimmune diseases, type I diabetes mellitus, and type IV hypersensitivity.

2. Materials and methods

2.1. Materials

Egg yolk lecithin-80 (E-80), cholesterol, distearoyl-sn-glycero-3-phosphoethanolamine-N- [maleimide (polyethylene glycol)-2000] (DSPE-PEG_{2000}-NH2) were obtained from Shanghai AVT Co., Ltd. ER-targeting polypeptide Pardaxin (PAR, sequence: H-GFFA-LIPKIISSPLFKTLLSAVGSALSSSGGQE-OH) was synthesized by Shanghai Qiang Yao Biotech Co., Ltd. DSPE-PEG_{2000}-PAR was obtained by a condensation reaction between the amino group of DSPE-PEG_{2000}-NH_2 and the carboxyl group of pardaxin polypeptide [21]. WST-1 cell proliferation and cytotoxicity assay kit, ER-Tracker Green and Hoechst 33342 were provided by Beyotime Co., Ltd. Cell Counting Kit-8 (CCK-8) was purchased from GLPBIO, USA. DiD perchlorate were from Dalian Meilun Biotech Co. Ltd. Ovalbumin (OVA, CAS: 9006-59-1) was from Fankew Chemical, and CpG ODN 1826 (sequence: 5′-T*C*C*A*T*G*A*C*G*T*T*C*C*T*G*A*C*G*T*T-3′) was synthesized by Shanghai Sangon Biotech Co., Ltd. Anti-mouse CD3e Ab (clone: 145-2C11), anti-mouse CD28 Ab (clone: 37.51), and recombinant mouse IL-2/-7 used for T cell activation and culture, together with FITC-conjugated anti-mouse CD3 (100204), PE-conjugated anti-mouse CD8a (100708), APC-conjugated anti-mouse CD62L (104412) and Percp-Cy5.5-conjugated anti-mouse/human CD44 (103032) antibodies that are used for flow cytometric studies were from Biolegend (San Diego, USA). Mouse IFN-γ (EK280HS), IL-2 (EK202HS) and IL-4 (EK204HS) high sensitivity ELISA kits were obtained from Multi-Sciences (Lianke) Biotech Co., Ltd. (Hang Zhou, China). Rabbit anti--β-actin antibody, HRP-anti-rabbit IgG (H + L), BCA protein assay kit, RIPA lysis buffer, and protease inhibitor cocktail were acquired from Biotechnology (Jiangsu, China), and HRP-goat anti-mouse-IgG (H + L) was from Yeasen Biotech Co., Ltd. Phosphatase inhibitor Cocktail II (ab201113) and rabbit anti-XBP1 antibody (EPR22004, ab220783) was purchased from Abcam. Rabbit anti-phospho-PERK (Thr982) antibody (DF7576) was from Affinity Biosciences, anti-β-actin monoclonal antibody and Alexa Fluor 488 Goat-anti-Rabbit IgG(H + L) secondary antibody was from Dakewe Biotech Co., Ltd. (Shanghai, China). Rabbit-anti-NF-kB p65 (10745-1-AP), ant-NFAT-c2 (22023-1-AP), and JUN (24909-1-AP) polyclonal primary antibody were from Proteintech Group, Inc., while CHOP (L63F7) mouse mAb #2895 was from Cell Signaling technology. ImunoSep™ mouse $CD8^+$ cell positive selection kit was purchased from Precision BioMedicals Co., Ltd. (Tianjin, China). KIRA6 (CAS: 1589527-65-0), ISRIB (trans-isomer, CAS: 1597403-47-8), GSK2606414 (CAS: 1337531-36-8), and Tacrolimus (FK506, CAS: 104987-11-3) were from MedChemExpress Co., Ltd. (New Jersey, USA). RPMI 1640 medium (RPMI) and penicillin-streptomycin (100 U/mL) were from JiNuo Biotechnology Co. Ltd. (Zhejiang, China). Fetal bovine serum (FBS) and 0.25% trypsin with 0.02% ethylenediaminetetraacetic acid (EDTA), sodium pyruvate, L-Glutamine, and non-essential amino acids (NEAA) was purchased from Gibco (Thermo Fisher Scientific. USA). Sterile absorbable surgical suture (4-0) for graft were from Shanghai Pudong Jinhuan Medical Products Co., Ltd. (Shanghai, China). Trichloromethane ($CHCl_3$), dimethyl sulfoxide (DMSO), Trichloroacetaldehyde hydrate (chloral hydrate) and formaldehyde (CH_2O) were purchased from Sinopharm Chemical Reagent Co., Ltd. The deionized water used was prepared using a Milli-Q system (Millipore, Boston), and all the reagents were of analytical grade.

2.2. Cell lines and animals

Murine lymphoma E.G7-OVA cells genetically engineered to synthesize and secret OVA constitutively were obtained from BeNa Culture Collection (BNCC, Beijing, China), while human acute T lymphocyte leukemia cell line Jurkat T were obtained from Shanghai Cell Bank, Chinese Academy of Sciences. E.G7-OVA and Jurkat T were cultured in complete RPMI 1640 medium (10% FBS, 1% penicillin-streptomycin). Mouse splenic lymphocytes and naive $CD8^+$ T cells were isolated and purified from spleen, and were cultured in complete 1640 supplemented with 2 mM L-Glutamine, 10 mM NEAA, 1 mM sodium pyruvate, and 50 mM β-mercaptoethanol at 37 °C in a humidified atmosphere containing 5% CO_2 (Heraeus, Germany).

Female C57BL/6 mice ($H\text{-}2K^b$) and BABL/c mice ($H\text{-}2K^d$) (Slaccas Experimental Animal Co., Ltd. Shanghai, China) used at 8–10 weeks of age were bred and maintained under pathogen-free conditions. All experimental procedures were conducted according to the protocols approved by the Institutional Animal Care and Use Committee of Zhejiang University.

3. Methods

3.1. Preparation and characterization of UPRi-loaded liposomes

UPR branch-specific small molecule inhibitor (UPRi)-loaded liposomes with or without ER-targeting capacity were prepared using thin-film rehydration method, and named as UPRi@lipoT and UPRi@lipoN, respectively. For UPRi@lipoT, lipid mixtures composed of E80, cholesterol, DSPE-PEG_{2000}, DSPE-PEG_{2000}-PAR (cholesterol: phospholipid = 1 : 4, m/m), together with hydrophobic UPRi were dissolved in the mixed solvent of ethanol and chloroform, and evaporated under reduced pressure to make a thin film of lipids. Subsequently, liposomes were prepared by probe ultrasound following the hydration of lipid film with deionized water. Similarly, UPRi@lipoN was prepared with an equivalent molar amount of DSPE-PEG_{2000} substituting for DSPE-PEG_{2000}-PAR.

The particle size and zeta potential of liposomes were measured with Dynamic Light Scattering (Malvern Zetasizer Nano-ZS instrument, UK). Meanwhile, their morphologies were observed under Transmission Electron Microscopy (TEM, JEOL JEM-1230 microscopes, Japan). After

removing free drugs by Sephadex G50 column, encapsulated ones were extracted with proper solvent following demulsification, and the encapsulation efficiency (EE %) was determined by UV–Vis absorption spectroscopy. Besides, cytotoxicity (24 h) of each preparation toward different cell lines were evaluated by WST-1 or CCK-8 assay according to the manufacturer's instructions.

3.2. Isolation, purification and bulk culture of T cells

Murine splenic lymphocytes (SPLCs) were collected, disposed with ice-cold erythrocyte lysis buffer, and further purified using magnetic microbeads separation (negative enrichment by $CD8^+$ MACS cell selection kit) to obtain naive $CD8^+$ T cells if necessary. Subsequently, SPLCs or sorted naive T-8 were cultured in anti-CD3e Ab (5 μg/mL) coated 24-well plates as 1×10^6 cells per well in 1 mL complete RPMI 1640 medium supplemented with anti-CD28 Ab (2 μg/mL), mouse recombinant IL-2 (10 ng/mL) and IL-7 (2 ng/mL) for 48 h. Afterwards, half medium were replenished with fresh medium containing cytokines every day. And cells were harvested for analysis after another 48–72 h. And to determine the kinetics of activation-induced cell expansion (Fig. S1), cells were collected at indicated time points and counted using cell counting chamber or flow cytometry (ACEA NovoCyteTM).

3.3. Cell uptake and subcellular co-localization

In order to investigate the endocytic behavior of lymphocytes, DiD was introduced to noncovalently label the hydrophobic part of liposome (DiD@lipoN and DiD@lipoT), while Hoechst 33342 was used for visualizing the nucleus. In brief, SPLCs were seeded into 24-well culture plate at a density of 5×10^5 cells in 1 mL complete medium per well, and subsequently treated with DiD@lipoN or DiD@lipoT for 1, 3, 6, 9, 24, 48 or 72 h (0.2 μg/mL DiD). Cells were collected, washed twice with phosphate buffer saline (PBS), postfixed with 4% formaldehyde for 10 min, and stained with Hoechst 33342 (10 μg/mL) for 30 min at room temperature. After extensive wash with PBS, SPLCs were seeded back into the plate and settled for 30 min. Afterwards, multi-channel photos were captured sequentially on the same focal plane under constant laser intensity with an inverted fluorescence microscope (AIR, Nikon, Japan), and further analyzed using graphic processing software Image J to semi-quantitate the fluorescence intensity of liposome to cell count. In addition, fluorescent pictures under same field of vision were merged by software EZ-MET.

To further validate the ER targeting ability of lipoT [21,22], the intracellular co-localization of lipoN/lipoT, ER and nucleus was investigated. SPLCs were seeded and treated with different preparation (DiD-lipoN and DiD-lipoT) for 48 h. Then, ER and nucleus were successively labeled with corresponding fluorescent dye (ER-Tracker Green and Hoechst 33342, respectively) according to the manufacturer's instructions. Next, cells were washed with PBS and fixed with 4% paraformaldehyde. Multi-channel photos were captured with an inverted fluorescence microscope (Nikon, Japan), and were analyzed using Image J and EZ-MET.

3.4. Quantitative analysis by flow cytometry and ELISA

Lymphocytes from primary tissues were harvested, erythrolysized, suspended in PBS (10^6 cells in 100 μL PBS), and incubated with suggested amount of fluorochrome-labeled anti-mouse antibodies against CD3, CD8, CD44, and CD62L for 45–90 min in dark at 37 °C. Then, cells were washed twice with ice-cold PBS to remove free antibodies and resuspended in fresh PBS for flow cytometric detection (BD Fortessa). And data were further analyzed with FlowJo V10 software.

The supernatant of cell culture was collected and condensed by freezing-thawing method if necessary. Blood sample was collected and centrifuged (2000 rpm, 10 min) with the upper serum carefully collected. And cytokine (IFN-γ, IL-2, IL-4) content was determined by high sensitivity ELISA kits as detailed in the manufacturer's instructions.

3.5. Western blot

Cells were harvested in ice-cold PBS at indicated time points, and lysed with RIPA buffer supplemented with phosphatase and protease inhibitor cocktail for whole lysate isolation. Subsequently, proteins were electrophoresed by SDS-PAGE, transferred to polyvinylidene fluoride (PVDF) membranes, blocked with 5% bovine serum albumin (BSA), sequentially incubated with corresponding primary antibodies and HRP-conjugated goat anti-rabbit/-mouse secondary antibodies. The protein bands were detected by an enhanced chemiluminescence (ECL) system (Bio-Rad). Antibodies used here include: rabbit anti-XBP1 (1:1000, XBP-1s: 56 kDa), phospho-PERK (Thr982) (1:2000, 125 kDa), β-actin (1:1000, 42 kDa), NF-kB p65 (1:1000, 65 kDa), NFAT-c2 (1:1000, 135 kDa), and JUN (1:1000, 39 kDa), mouse anti-CHOP (1:1000, 27 kDa), and HRP-anti-rabbit IgG (H + L) (1:2000), or peroxidase affiniPure goat anti-mouse IgG (H + L) (1:5000). Semi-quantitative analysis was performed with Image J.

3.6. Immunofluorescence staining

The expression of NF-kB p65, NFAT-c2 and JUN (AP1) by SPLCs were analyzed using immunofluorescence assay following the manufacturer's instructions. Briefly, isolated SPLCs were treated separately with RPMI-1640, KIRA6@lipoT (1.5 μM), FK506@lipoN (5 nM), and KIRA6@lipoT (1.5 μM) plus FK506@lipoN (5 nM) for 24 h at 37 °C. Cells were then washed with PBS, fixed with 4% paraformaldehyde for 10 min, permeabilized with 0.2% Triton X-100 for 10 min, and blocked with 10% FBS in PBS for 60 min. Afterwards, they were incubated with anti-NF-kB p65 (1:200), anti-NFAT-c2 (1:100) or anti-JUN (1:50) primary antibody overnight at 4 °C, followed by an incubation with Alexa Fluor 488-conjugated goat anti-rabbit IgG (H + L) (1:300) secondary antibody for 1 h at room temperature. After labeled with Hoechst 33342, cells were visualized using fluorescence microscope. And Image J was used to semi-quantitate the fluorescence intensity.

3.7. In vitro and in vivo administration

3.7.1. In vitro

Different UPRi (KIRA6 inhibits the activity of IRE1α RNase and Kinase, GSK2606414 inhibits the phosphorylation of PERK, while ISRIB reverses the translational effects elicited by phosphorylation of eIF2α)-loaded liposomes were administered to SPLCs or sorted naïve T-8 at their activation phase (i.e., the first 48 h that under TCR stimulation), expansion phase (i.e., the following 48 h without TCR activation), or both phases. And the final concentration of each drug was selected referring to their cytotoxicity (1.5 μM KIRA6, 200 nM ISRIB, 200 nM GSK2606414).

3.7.2. In vivo

Prophylactic vaccination In order to evaluate the effect of UPR in unstressed physiological condition, C57/BL6 mice were randomly divided into five groups (n = 5), and subcutaneously injected with 100 μL PBS, or equal volume of PBS solution containing OVA + CpG, (OVA + CpG)@lipoN, or (OVA + CpG)@lipoT near the draining inguinal LNs (dLNs). Such vaccination was performed three times with an interval of 7 days. And in the group with UPR meddling, KIRA6@lipoT was administered three days after each vaccination (s.c., near dLNs). Here, 100 μg OVA, 25 μg CpG, and 0.2 mg KIRA6 were used for each mouse. And 16 days after the third immunization, mice were challenged with E.G7-OVA tumor cells (6.5×10^5 cells each mouse, s.c., at the right flank). Another 20 days later, mice were sacrificed with their peripheral blood, inguinal lymph nodes (LNs), and spleen collected for flow cytometry analysis, orthotopic tumor and axillary LNs collected for analyzing the infiltration of T-8 and the secretion of IFN-γ, and inguinal LNs embedded

in paraffin for H&E staining. Body weight and tumor volume of each mice were recorded every other day (tumor volume = length × width × height/2). The fluorescence intensity of T-8 (red) and IFN-γ (green) to cell count was semi-quantitated with Image J, while the tumor growth curve, tissues weight, and survival curve were analyzed using Prism-GraphPad.

Therapeutic vaccination To further investigate the involvement of UPR in stressed pathological condition, C57/BL6 mice were randomly grouped (n = 8), and subcutaneously inoculated with E.G7-OVA cells (7×10^5 cells/mice) at the right flank. When the tumor volume reached some 50 mm^3, first immunization (with PBS, KIRA6@lipoT or KIRA6@lipoN, s.c., at dLNs, 0.2 mg KIRA6 for each mouse) was carried out. Such vaccination was performed every 7 days. And another 10 days after the third immunization, mice were sacrificed with their peripheral blood, inguinal LNs, and spleen collected for flow cytometry analysis.

3.7.3. Allogeneic skin transplantation

Full-thickness trunk skin allograft was performed with standard techniques [23]. Briefly, the back skin of euthanized (10% chloral hydrate, i.p.) donor (C57BL/6) was carefully harvested with its hair shaved and the connective/fat tissues removed, which was later cut into 1-cm^2 pieces, and placed in ice-cold sterile PBS for later use. Subsequently, a 0.8-mm^2 square of skin was removed from the back of anesthetized recipient (BALB/c). Then, the graft from donor was placed atop the graft bed of recipient, followed by a continuous suture and careful trimming of excess donor skin. Afterwards, an adhesive bandage was used to cover and protect the surgical site.

Recipients were randomly grouped (n = 6), and subcutaneously administrated with 100 μL PBS, or equal volume of PBS containing lipoN, lipoT, KIRA6@lipoN, KIRA6@lipoT, FK506@lipoN, or KIRA6@lipoT plus FK506@lipoN near bilateral inguinal dLNs. Such administration was performed every four days from the day of transplantation, where 2 mg/kg FK506 and 10 mg/kg KIRA6 were used for each mouse. And on the 7th day, mice were sacrificed with their peripheral blood, LNs (axillary and inguinal), and spleen collected for flow cytometry analysis, serum IFN-γ, IL-2 and IL-4 determined by high ELISA kits, transplanted skin collected for investigating the infiltration of T-8 (pink) and $CD80^+$ (green) CD11c+ (red) antigen presenting cells, and evaluating the histological changes of grafts using H&E staining. And LNs were partially used for investigating the expression of XBP1+ (green) T-8 (red). And such experiment was repeated for another time, when the grafts were visually scored (Table S1) every two days for evidence of rejection. Here, according to the necrotic degree of donor tissue, scores were made where 0, 1, 2, 3, 4 and 5 corresponded to intact graft, first clear signs of graft rejection, > 25% rejection, > 50% rejection, > 75% rejection, and >90% rejection, respectively (referring to Schwoebel F et al. [24]). Once scored 5, the transplanted skin was regarded as undergoing complete rejection. Meanwhile, the body weight of mice was recorded daily as an assessment of their overall health.

3.8. Statistical analysis

Data were represented as mean ± standard error. Comparisons between two or several groups were analyzed using unpaired student's t-tests or one-way analysis of variance (one-way ANOVA, Tukey's multiple comparisons test), respectively. To conduct the best possible analysis of results from the cell uptake and colocalization investigations, all experiments were performed independently at least three times. All presented data are representative. The fluorescent images were viewed, processed, and analyzed by Image J. All statistical analyses were carried out by Prism-GraphPad version 7 Software (San Diego, CA), with a value of $P < 0.05$ considered to be statistically significant.

4. Results

4.1. UPR is ubiquitously expressed in hematopoietic cells and participates the activation-induced phase transition of T-8

UPR orchestrates both innate and adaptive immunity, supporting the maturation [18] and stress-response [12,27] of immune cells. Raw microarray data from *Bloodspot* reveals the transcriptional profiling of key UPR members in hematopoietic cells at their different maturation stages [25,26,28]. In particular, protein folding ER chaperone BiP (encoded by HSPA5) was highly expressed in almost all subpopulations, while pro-apoptotic ATF4 and CHOP (encoded by Ddit3) were universally low expressed, possibly constituting the cellular intrinsic resilience against perturbation. On the other hand, UPR members are ubiquitously high-expressed in lymphocytes, dendritic cells, and monocytes (Fig. 1A), which is consist with the research disclosure that UPR supports the development and physiological activities of these cells [13,19,27]. By contrast, a lower expression is observed in T-8 subsets (Fig. 1A). However, upon activation (OT-I mice antigen-specifically infected with OVA-expressing Listeria monocytogenes (Lis-OVA), and harvest the splenic T-8 at indicated time points for analysis in this case), ATF6 is readily up-regulated and maintains high expression. Similarly, IRE1 (ERN1) is remarkably induced 2 days post infection with a persistent up-regulation aftermath. Meanwhile, PERK (EIF2AK3) is down-regulated to a certain extent all along (Fig. 1B). Concurrently, XBP1, BiP, Eif2a and ATF4, key downstream molecules of UPR, are upregulated upon activation, although at varying degrees. But they restore basal expression over time. Interestingly, CHOP displays a quite opposite mode of response, which is firstly down-regulated and latter levelled up (Fig. 1C). Moreover, in this model, the expression of CHOP exceeds its basic value from day 6 (Fig. 1C), when the upstreaming PERK also undergoes a short-term up-regulation (Fig. 1B), which further confirms the direct correlation of UPR participants.

Under immunological stimulation, T-8 extensively proliferate, which is accompanied by a massive secretion of cytokines (IL-2, IFN-γ, TNF-α, etc.) and effector molecules (perforin, Granzyme, etc.), increased cytoplasmic Ca^{2+}, and aggravated intracellular oxidative stress, leading to an activation of UPR. IRE1 and ATF6 axes mainly function to facilitate cellular adaptability, exhibiting rapid up-regulation at the early responding stage. At the same time, downstream effector molecules (XBP1, BiP, etc.) are efficiently activated to alleviate ER stress and restore homeostasis, and they gradually resume in pace with the clearance of antigenic substance. However, UPR sensors IRE1 and ATF6 were irreversibly up-regulated, which may endow surviving memory cells with higher resistance to stress stimulus, so as to withstand a robust recall response. On the other hand, PERK has pleiotropic signaling outcomes. And upon acute stress insult, PERK demonstrates more inclination to elicit apoptosis. Thus, a limited expression of PERK might facilitate the survival of cells. Meanwhile, ATF4 and Eif2a, downstream of PERK, display a reversible early up-regulation, leading to a translational interception to curb the unrestrained ER protein inflow. And the pro-apoptotic CHOP is activated at a later stage, possibly to mediate the large-scale apoptosis of short-lived terminal effector cells (Tsle) that are highly sensitive to apoptotic stimulation during contraction phase [29], contributing to the quantity, quality and diversity of T-lymphocytes. Therefore, it can be speculated that naive T-8 proliferate and differentiate under activation, giving rise to heterogeneous T-8 subsets, in which Tsle are sensitive to apoptotic stimulation, and is eliminated during contraction, while memory precursor T cells (Tmp) survive to gain a higher expression of IRE1 and ATF6, equipped with better adaptability to provide long-term immunoprotection.

In brief, these gene signatures confirm that UPR is widely expressed in hematopoietic cells, including lymphocytes, and UPR participates the activation-induced phase transition of T-8.

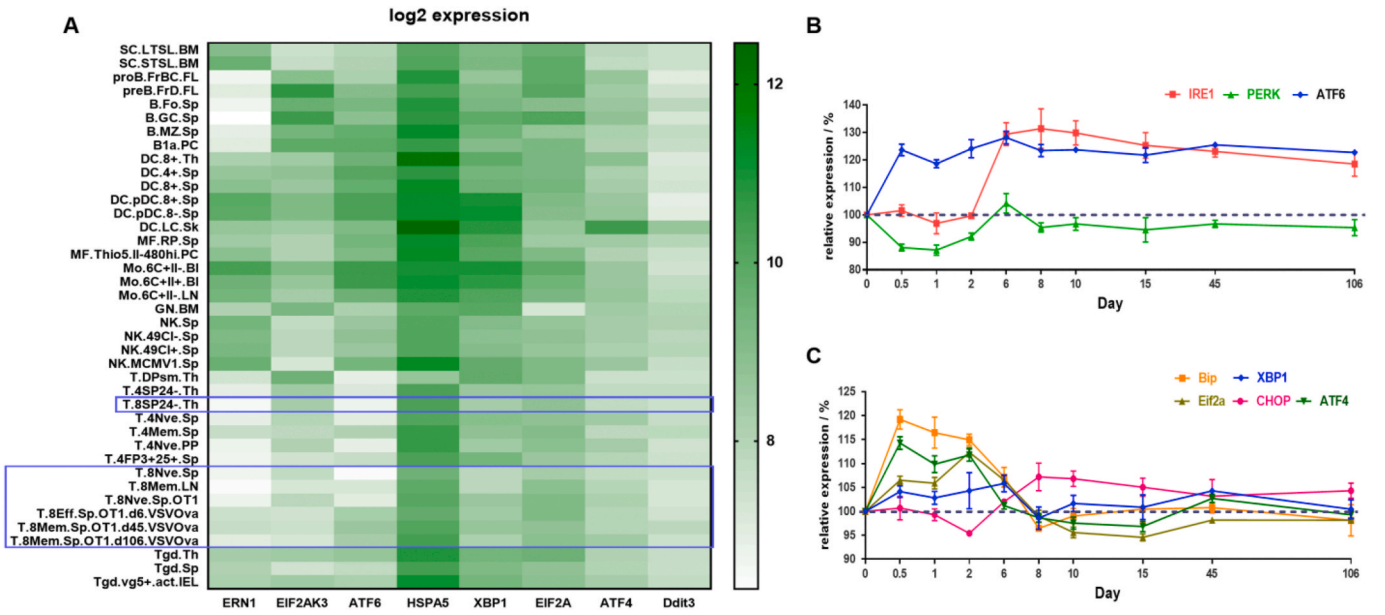

Fig. 1. UPR-associated gene signatures in murine hematopoietic cells. (A) Heatmap of differentially expressed genes (RNA-seq data) related to UPR-predominant members in mouse Immunological Genome Project (ImmGen) key populations at different maturation stages based on curated oligonucleotide microarray data. T-8 associated gene expression in the clustered heatmap is highlighted with blue box. (B-C) Relative mRNA expression of UPR-associated genes: ERN1 (IRE1), EIF2AK3 (PERK), ATF6 in (B), and HSPA5 (Bip), XBP1, EIF2A (Eif2a), Ddit3 (CHOP), ATF4 in (C) by LisOVA-infected OT-I T-8 with time. BM: bone marrow, FL: fetal liver, Sp: spleen, PC: peritoneal cavity, Th: thymus, Sk: skin, LN: subcutaneous lymph node, PP: peyers patches, IEL: intestine, Fo: follicuilar, GC: germinal center, MZ: marginal zone, RP: red pulp, SC: stem cell, LT: long-term, ST: short-term, DC: dendritic cell, pDC: plasmacytoid DC, Mo: classical monocytes, GN: neutrophils, DP: double-positive, SP: single-positive, T.4: CD4, FP3+25+: $CD25^{+}$ Foxp3+ Tregs, T.8: CD8, Nve: naïve, Mem: memory, Eff: effector, Tgd: thymic TCRgamma-delta, act: activated. Raw microarray data and more detailed information is available from *Bloodspot* [25,26] (http://servers.binf.ku.dk/bloodspot/, accession number: GEO: microarray data, GSE15907). (For interpretation of the references to colour in this figure legend, the reader is referred to the Web version of this article.)

4.2. The preparation and characterizations of UPRi-loaded ER-targeting liposome

In view of the intricate intersections among UPR members and the pleiotropic effects of UPR in mediating a cross talk between survival and perish [30–32], a fine tuning over the target and degree of UPR is of great importance. Small molecular drugs are easy to use, with high biosafety and superior site-selectivity, which provides a platform for meticulously and specifically regulating UPR branches. However, most molecules themselves cannot efficiently penetrate the cell membrane, let alone reach their intracellular site of action. In addition, the solubilization by cosolvent may cast certain cytotoxicity to cells, especially to the high sensible T-8 subsets. And to achieve an expected efficacy, such low accessibility is usually compensated by an increased dosage, which may add up ER load, and even complicate cellular response, leading to an altered stress response. Capable of efficacy-enhancing and toxicity-reducing, pharmaceutical strategies are extensively used to promote the regulatory precision by increasing site-selective accumulation. As most molecules interact with their corresponding receptors located at specific intracellular site, a targeted delivery over subcellular organelle might be more promising. Considering the fact that all three UPR transducers (IRE1α, PERK, and ATF6) reside in ER membrane, we believe that an ER-targeted delivery of molecules specific for UPR sensors may alter the intracellular trafficking and utilization of drugs, favoring an objective output of investigation.

Based on our previous studies on ER-targetable nanocarriers [21,22], lipophilic ATP-competitive IRE1α Kinase Inhibiting RNase Attenuator 6 (KIRA6) [33,34]-loaded liposomes with or without ER-targeting capacity were prepared, and named as KIRA6@lipoT and KIRA6@lipoN, respectively (Fig. 2A), which had a particle size of 100–150 nm, zeta potential at -20-0 mV (Fig. 2B), drug encapsulation rate over 80% (Table S2), displaying typical bilayer vesicle structures (Fig. 2C), and low cytotoxicity towards quiescent or α-CD3/-28 Abs-activated SPLCs at a concentration up to 15 μM (24h) (Fig. 2D). When the fluorescent probe DiD was used as model cargo, the *in vitro* uptake of DiD@lipoN and DiD@lipoT by SPLCs peaked at 48 h, when the ER-targetable group outplayed with significantly higher DiD fluorescent intensity (Fig. 2E–F), which might owe to the liposomal surface modification of Pardaxin, an ER-targeting cationic polypeptide with membrane-permeability and non-lysosomal intracellular trafficking [21]. Interestingly, lymphocytes, especially activated ones (as well as tumor cells that features extensive proliferation and secretion (Fig. S2)), exhibited higher sensitivity to KIRA6@lipoT treatment (Fig. 2D). A possible explanation might be that ER-targeting nanocarriers promote the endocytosis of cells (Fig. 2E–F) and facilitate the site-specific inhibition of KIRA6 (Fig. 2G). Activated lymphocytes or malignant cells with active biological activities bear heavier ER burden and thus own higher dependency on UPR, manifested as a lower tolerance to IRE1α inhibition. These findings indicate that lymphocytes under different physiological conditions (quiescent or activated) vary in their dependence on UPR.

4.3. Lymphocytic IRE1α inhibition induces a systemic immunosuppression

Activated immunity is usually accompanied by an up-regulated stress responses in multiple immunocytes, and repressing lymphocytic UPR might impair the overall immunity. In order to verify our hypothesis, mice anti-tumor model was used for monitoring the systemic immunity [35], with easy operation, intuitive observation and multifaceted measurement indicators.

Firstly, to explore the immunosuppressive effect of lymphocytic IRE1α inactivation in unstressed physiological condition, a prophylactic anti-tumor vaccination model was established (Fig. 3A). It was suggested that antigens directly delivered to the ER of antigen presenting cells (APCs) facilitated the development of cross-presentation [36–38], and our results suggested that ER-targetable (OVA + CpG)@lipoT did display certain anti-tumor potential (Fig. 3B), with an increased T-8 infiltration and IFN-γ secretion both in LN and orthotopic tumor

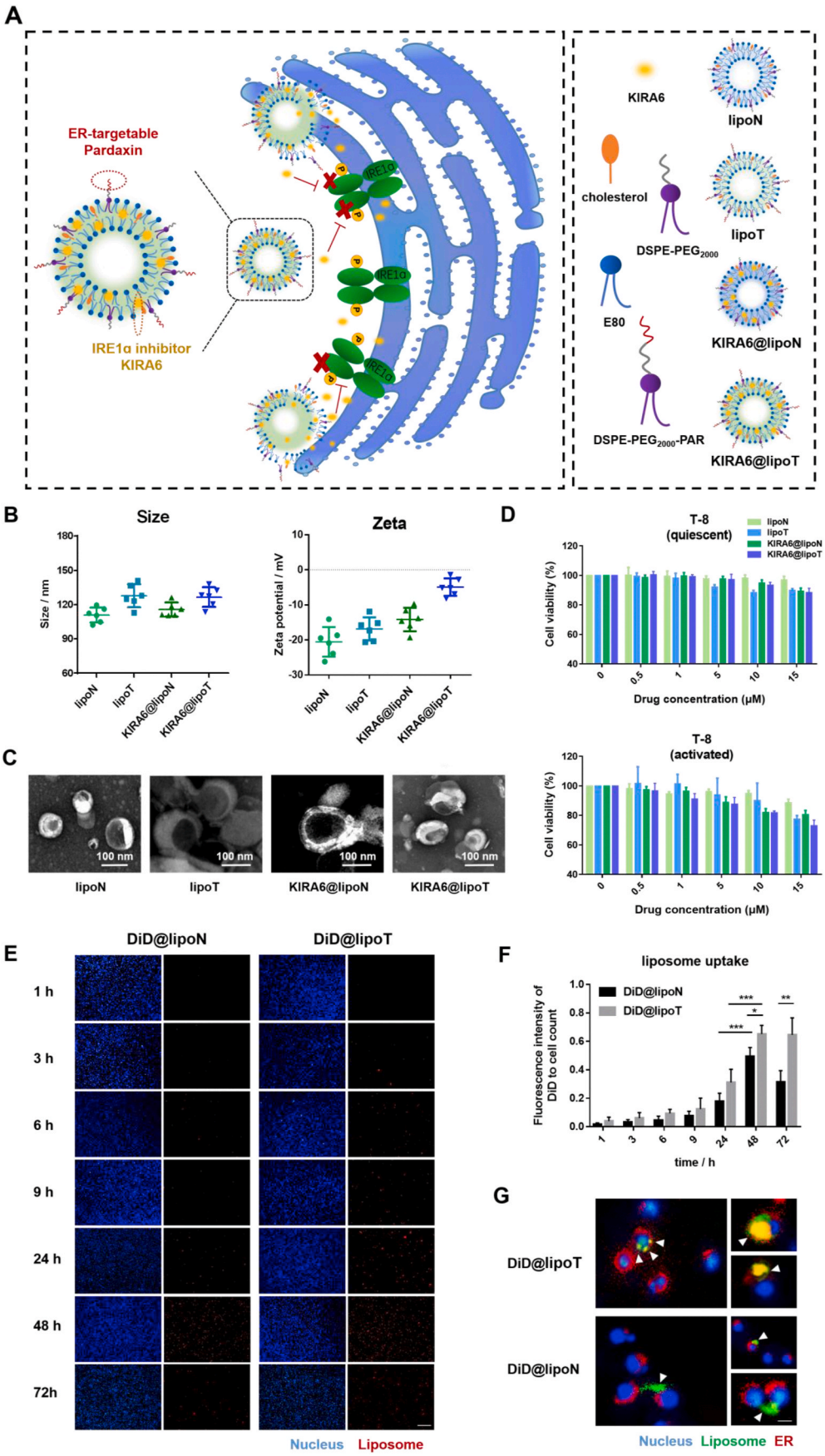

Fig. 2. Preparation and characterizations of KIRA6-loaded liposome. (A) Schematic diagram illustrating the structure and composition of lipoT, lipoN, KIRA6@lipoT, and KIRA6@lipoN, together with the action mode of KIRA6@lipoT. (B) Particle size and zeta potential of different liposomal preparations, n = 6. (C) TEM images of different liposomes. Scale bar, 100 nm. (D) Cell viability of quiescent (naive) or activated (α-CD3/28 Abs stimulation) splenic T-8 incubated with different liposomes at varying drug concentration for 24 h, respectively, n = 5. (E-F) Cellular uptake of DiD@lipoN and DiD@lipoT. Fluorescence images (E) were taken at 1, 3, 6, 9, 24, 48 and 72 h, respectively. Scale bar, 200 μm. Fluorescent images from four randomly select fields of view were processed, and analyzed by Image J to semiquantitate the fluorescence intensity of DiD (F). All error bars were expressed as ± SD, *$p < 0.05$, **$p < 0.01$. Data are representative of multiple independent experiments. (G) Typical images displaying the intracellular co-localization of ER, liposome and nucleus in SPLCs treated with DiD@lipoN or DiD@lipoT for 48 h. Blue stands for nucleus, with red for ER, green for DiD-labeled liposome, and orange for the co-localization of liposome and ER (arrow). Scale bar, 3 μm. (For interpretation of the references to colour in this figure legend, the reader is referred to the Web version of this article.)

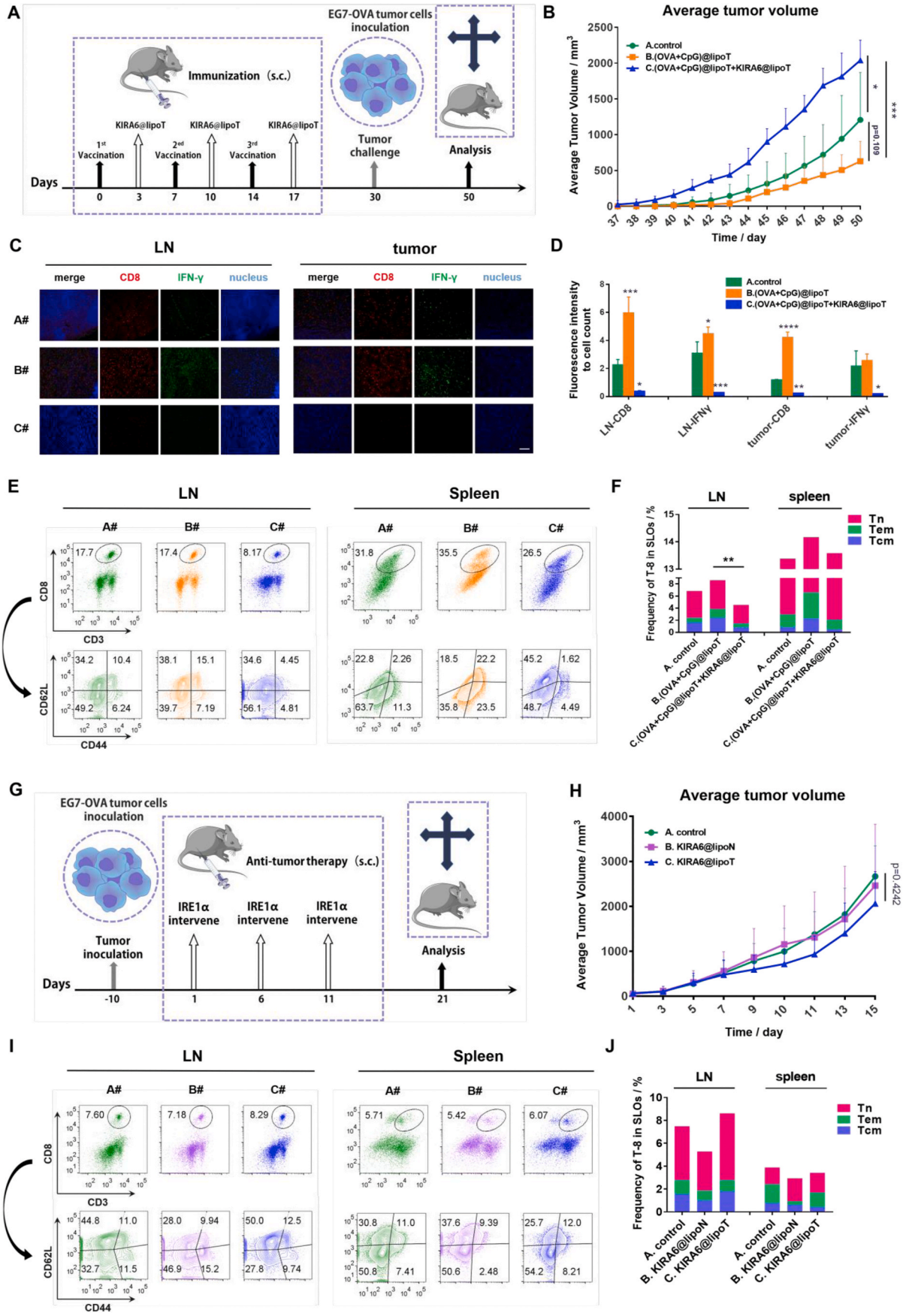

(caption on next page)

Fig. 3. Prophylactic and therapeutic vaccination *in vivo*. (A) Experimental scheme of prophylactic vaccination, n = 5. (B) Tumor growth curve of mice in different groups. (C-D) Representative immunofluorescence images (C) of orthotopic tumor and axillary LN from each group (blue-nucleus, red-CD8, green-IFNγ). Quantitative analysis of fluorescent positive cells was shown in (D), n = 3. Scale bar, 200 μm. (E-F) Representative flow cytometric pictures (E) and summary plot of data (F) showing the frequency of T-8 ($CD3^+$ $CD8^+$ subset), $CD8^+$ Tem ($CD3^+$ $CD8^+$ $CD44^+$ CD62L-), $CD8^+$ Tcm ($CD3^+$ $CD8^+$ $CD44^+$ CD62L+) and $CD8^+$ Tn ($CD3^+$ $CD8^+$ $CD44^-$ CD62L+) in LN and spleen, n = 4. (G) Experimental scheme of therapeutic vaccination, n = 7. (H) Tumor growth curve of mice in different groups. (I-J) Representative flow cytometric pictures (I) and summary plot (J) showing the frequency of T-8, $CD8^+$ Tem, $CD8^+$ Tcm and $CD8^+$ Tn in LN and spleen, n = 4. All error bars are expressed as ± SD, *p < 0.05, **p < 0.01, ***p < 0.001 and ****p < 0.0001. (For interpretation of the references to colour in this figure legend, the reader is referred to the Web version of this article.)

(Fig. 3C–D). However, when used in combination with KIRA6@lipoT, the anti-tumor effect of (OVA + CpG)@lipoT was totally reversed, as the tumorigenesis (Fig. 3B) and metastasis (Fig. S3) was significantly promoted. Further investigation indicated that IRE1α inhibition remarkably reduced the frequency of T-8 in secondary lymphoid organs (SLOs, LN and spleen in this case), and the proportion of effector memory T cells (Tem) and central memory T cells (Tcm) in these T-8 were also significantly down-regulated (Fig. 3E–F). These results provide direct evidence that under normal physiological conditions, the intervention of lymphocytic IRE1α induces a systemic immunosuppressive environment, which is partially through a negative regulation over the quantity, function and memory differentiation of T-8.

Next, we sought to further investigate the immunological inhibition of lymphocytic IRE1α inactivation at stressed pathological settings, where a therapeutic anti-tumor vaccination model was used (Fig. 3G). Intriguingly, the inhibition of IRE1α showed no significant tumor-promoting effect this time (Fig. 3H). And flow cytometric results suggested that the proliferation and memory commitment of T-8 in SLOs were not significantly altered (Fig. 3I–J). Considering that malignant cells can obtain stronger tumorigenicity, metastasis and drug resistance via UPR [39], and there's certain cytotoxicity of IRE1α inactivation to tumor cells (Fig. S2), as well as the fact that tumor-bearing mice already established immunosuppression, we believe that these results are more likely to be derived from a complexed inhibition effect of KIRA6 against both tumor cells [39] and immune cells [13,14,40]. Generally speaking, suppressing IRE1α axis of lymphocytes reshapes immunoenvironment, resulting in an impaired systemic immunity.

4.4. Lymphocytic UPR abrogation, especially at the activation phase, limits the priming, effector function and memory commitment of T-8

In the above section, results indicate a close correlation between lymphocytic UPR disturbance-derived immunosuppression and an altered T-8 biology. And liposomes were subcutaneously administrated near the draining LNs so as to enhance the pharmacological regulation over lymphocytes, which might be complicated by the sophisticated *in vivo* microenvironment. Therefore, *in vitro* investigations using SPLCs or sorted T-8 were carried out, which provided a more intuitive insight into the interrelationship between UPR and the bioactivities of lymphocytes, especially T-8.

Years of exploration unveils the molecular details of T-8 in epigenetics [41], transcriptomics [17], and translatomics [42]. And it's indicated that the pattern of T-8 phase transition is generally a stereotype [17]. Namely, following tripartite stimulation from cognate antigen, costimulatory signal and microenvironmental cues, naïve T-8 undergoes an unceasing process of activation, effector expansion, contraction and memory turnover. Effector T-8 proliferate extensively to generate massive clones with high cytotoxicity, orchestrating a rapid clearance of 'non-self' invaders. Meanwhile, memory T-8 that feature high resilience and robust recall response can provide a long-term immune surveillance. Here, according to the proliferative kinetics of SPLCs and T-8 following activation *in vitro* (Fig. S1), the first 2 days subjected to TCR stimulation is defined as the activation phase, considering the relatively mild quantitative growth; while the 3rd to 6th day with extraordinarily rapid proliferation is regarded as the expansion phase; the contraction phase is reached approximately at the 7th day as the proliferation flattened out, and it's speculated that the memory turnover phase may follow consequently. Considering that stimulation at the early responding stages plays a decisive role in triggering the developmental program of T cells [43,44], we believe that the activation and expansion phases are the 'causes', while the contraction and memory phases are the 'consequences'. Therefore, UPR intervention was mainly cast on the first two phases, with indicators characterizing the latter two phases analyzed, including the phenotype and quantity of T-8.

Based on our preliminary exploration, IRE1α inhibition, especially at the activation phase, impaired the quantitative scale and memory commitment of T-8 (Fig. S4), suggesting a stage-selective dependency of UPR. Here, we further investigated the participation and function of IRE1α and PERK signaling pathways in splenic lymphocytes, especially in T-8, at their activation phase, expansion phase, or both (activation plus expansion) phases (Fig. 4A), where KIRA6 (1.5 μM) inhibited the activity of IRE1α RNase and Kinase, GSK2606414 (200 nM) limited the phosphorylation of PERK, and ISRIB (200 nM) reversed the translational effects of p-eIF2α (Fig. 4K–L). Under the above dosage, there was no significant cytotoxicity of these preparations (Fig. S5), and a desirable target-inhibition was achieved, especially when inhibitors are delivered via ER-targetable liposome (Fig. 4K–L). It turned out that KIRA6 treatment limited the proliferation and memory differentiation of T-8, in which ER-targetable KIRA6@lipoT displayed higher efficiency than its non-targetable counterpart (KIRA6@lipoN). Moreover, the activation phase was more sensitive to IRE1α intervention than the expansion phase, and inhibiting both phases exhibited a highest negative regulation. In addition, similar results were observed using inhibitors of PERK axis (Fig. 4B–F), suggesting that UPR branches play a vital role in the activation-induced phase turnover of T-8. It is worth noting that both the frequency (Fig. S6) and quantity (Fig. 4D) of naïve T-8 increased remarkably upon IRE1α inactivation, which further confirmed that this pathway was indispensable for the transition of T-8 from resting state to activated state. Furthermore, the cytokine secretion by lymphocytes was meddled (Fig. 4G–J). Specifically, inhibiting UPR at the activation phase or both phases down-regulated the immuno-potentiating IL-2 and IFN-γ, but up-regulated the immunosuppressive IL-4. On the contrary, inhibition at the expansion phase up-regulated IL-4, IL-2 and IFN-γ concurrently, possibly due to an alleviation effect to the hyper-ER stress during extensive clonal expansion.

We believe that there is a phase-selective UPR participation, in which UPR dependence of each phase is: activation > expansion ? contraction > memory turnover. Likewise, a subset-differential stress tolerance may also exist, where the adaptability of different T-8 subgroup is: memory > naïve > effector > terminal effector, as depicted in Fig. 5.

4.5. Lymphocytic IRE1α inhibition contributes to a reduced skin allograft rejection

The above results suggest that under stimulation, lymphocytic IRE1α inhibition leads to an overall immunosuppression that is closely related to the limited activation, clonal expansion, effector function and memory commitment of T-8, which might be used to improve the pathophysiological manifestations of diseases and disorders caused by hyperactivated lymphocytes (especially T-8), including transplantation rejection [45–47].

Allogeneic skin graft suffers greatly from acute rejection that is mainly mediated by T-lymphocytes [48,49]. The high antigenicity and continuous exposure of allogeneic skin patch triggers allorecognition of

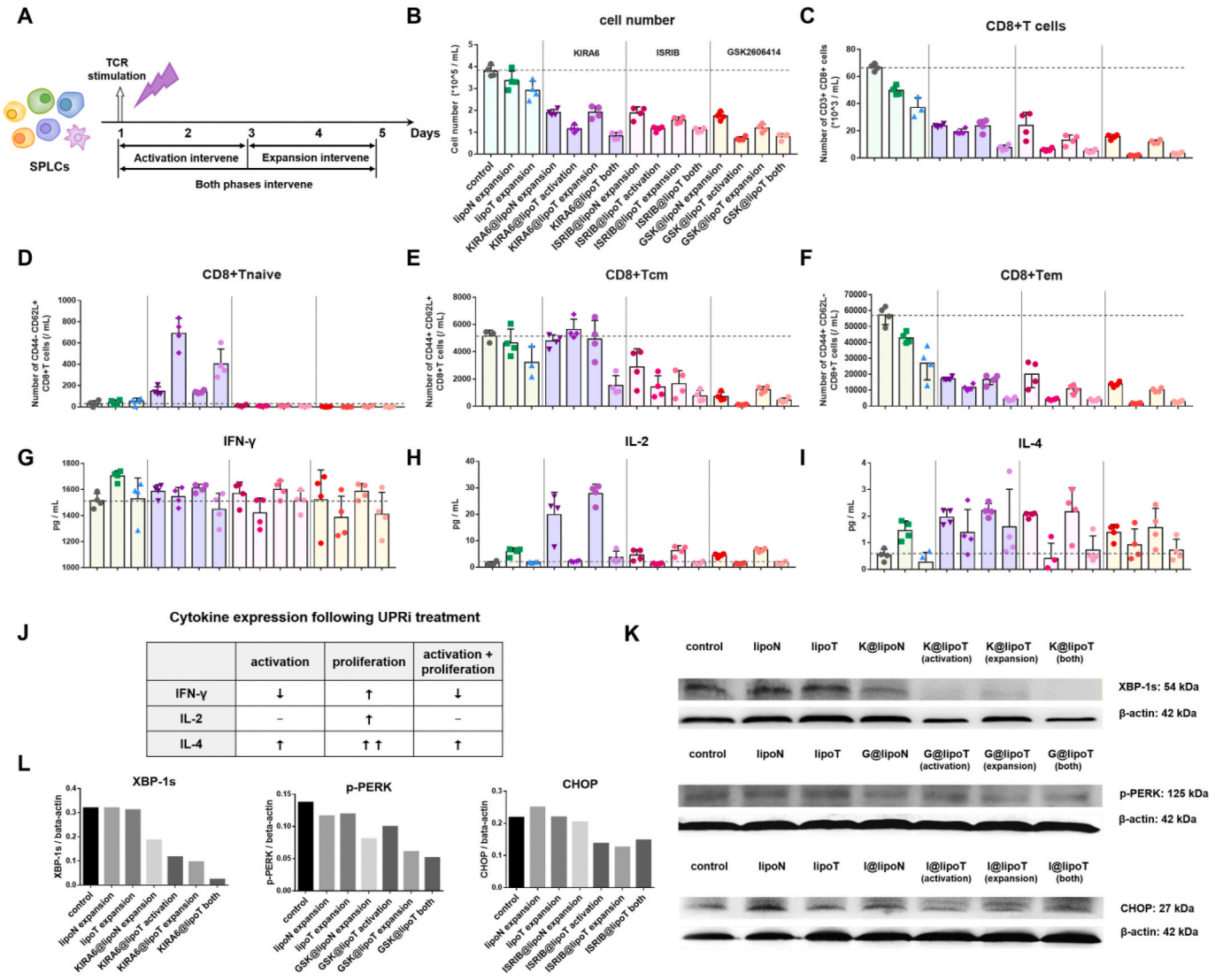

Fig. 4. The phenotype and quantity of T-8 under UPR intervention. (A) Schematic illustration of SPLCs treated with different preparations at the activation phase, expansion phase or both phases (1.5 μM KIRA6, 200 nM ISRIB, 200 nM GSK2606414). (B-F) Flow cytometric analysis of data showing the quantity of SPLCs (B), T-8 (C), $CD8^+$ Tn (D), $CD8^+$ Tcm (E), and $CD8^+$ Tem (F) under different treatments, n = 4. (G-J) Determination (G-I) and summary table (J) of the secretion of IFN-γ (G), IL-2 (H) and IL-4 (I) in culture supernatant using cytokine kits, n = 4. All error bars were expressed as mean ± SD. (K-L) Immunoblot analysis of XBP-1s, p-PERK and CHOP expression in T-8 treated with different UPRi-loaded liposomes at indicated phases.

recipient T cells. Subsequently, activated CD4+/CD8+ T cells launch an intensive host immune response that drives graft rejection [5,50]. At present, immunosuppressive therapy has little or no effect in allogeneic skin transplantation [49], while the development and application of artificial skin is challenged by a high cost and low feasibility. In these respects, skin transplantation is currently limited to autologous ones [51,52]. Murine allogeneic skin graft is a classic model for studying the cellular immunity-associated acute rejection [53], which is repeatable, easy to operate, and minimally affected by humoral immune response, where T-lymphocyte, especially T-8, are one of the main troublemakers involved in such rejection [5,50].

Widely used in organ transplantation and autoimmune diseases, FK506 (tacrolimus) is a calcineurin inhibitor approved by FDA for clinical use. FK506 binds with cytoplasmic immunosuppressive protein FKBP12 to form a complex that competitively interacts and limits the activity of calcineurin, inhibiting the dephosphorylation and nucleus translocation of nuclear factor of activated T cells (NFAT) ligand, thus curbing the activation of T cells [54]. Considering the poor water solubility (2–4 μg/mL) and low bioavailability (~18%) of FK506 [55], together with its specific site of action (cytoplasm), we loaded FK506 onto the non-ER targeting lipoN (FK506@lipoN). It's reported that a high dose of CaNIs may exert hepatotoxicity and kidney toxicity, yet no obvious toxicity to these organs was observed 7 days post grafting (Fig. S7), indicating a relatively high biosafety of our administration regimen (Fig. 6A). And it turned out that both FK506@lipoN and KIRA6@lipoT displayed limited rejection-alleviating efficacy, while the combined treatment significantly alleviated rejection, prolonged the graft survival (Fig. 6B–D), and maintained the structural integrity of transplanted skin (Fig. 6D and L, S7A), which was further confirmed by an impaired proliferation and memory generation of T-8 in SLOs (Fig. 6E–F), inhibited infiltration of APCs and T-8 in skin (Fig. 6J-L), and down-regulated IL-2 and IFN-γ, but up-regulated IL-4 in serum (Fig. 6G–I). In brief, lymphocytic IRE1α inhibition induced the suppression of overall immunity, contributing to a higher graft compatibility, which was associated with the limited effector and memory T-8. Moreover, there was a synergistic immunosuppressive effect of IRE1α inactivation and calcineurin inhibition, which displayed promising potential in rescuing allogeneic transplantation rejection.

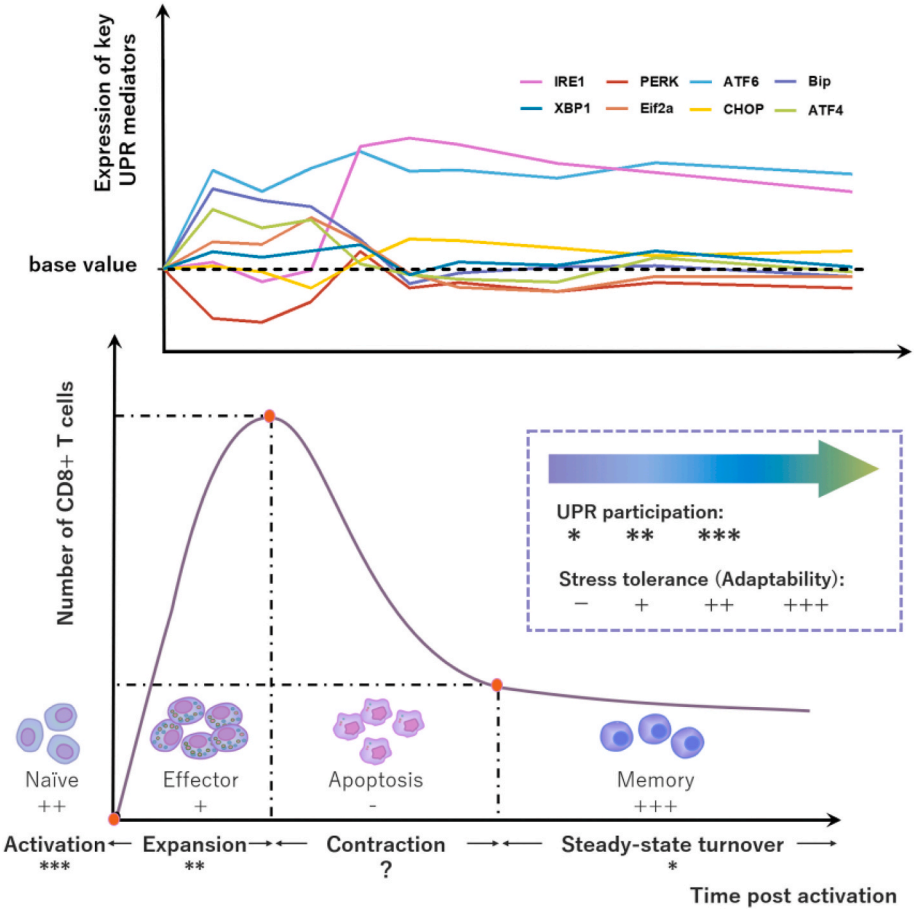

Fig. 5. Phase-selective UPR participation and subset-differential stress tolerance by T-8. n T-8, the gene expression mode of UPR bears much resemblance to the cellular proliferative kinetics upon activation stimulus. And it's postulated that there is a varying UPR dependence by different phases: activation > expansion ? contraction > memory turnover. Accordingly, the stress adaptability of different T-8 subsets is distinctive: memory > naïve > effector > terminal effector.

4.6. A cross-talk between inflammatory transcriptional factors and IRE1α axis

Inflammatory transcriptional factors (TFs) are indispensable for the priming of lymphocytes, which also facilitate the development of T cell-mediated transplantation rejection [56]. In particular, inhibiting activation-related inflammatory TFs such as NFAT, activator protein-1 (AP-1) and nuclear factor-κB (NF-κB) results in an immunosuppressive effect [57]. For instance, FK506 limits the activation of NFAT to reduce T cell-associated graft rejection and autoimmunity [54]. And it's reported that FK506 also partially inhibits NF-κB [58]. Increasing evidence suggests that UPR is intertwined with several inflammatory responses [59]. Under ER stress, IRE1α forms a complex with TNF receptor-associated factor 2 (TRAF2) at the kinase domain, which induces the phosphorylation of Jun N-terminal kinase (JNK) [60] and upregulates the expression of pro-inflammatory genes through AP-1 [61]. In addition, the IRE1α-TRAF2 complex recruits IκB kinase (IKK) to phosphorylate and degrade of IκB, releasing NF-κB for nuclear translocation [59,62].

ER stress triggers the homo-oligomerization and *trans*-autophosphorylation of IRE1α lumenal domain, which further drives the homo-oligomerization of its cytosolic kinase/RNase domains to activate this signaling pathway. KIRA6 is an ATP-competitive IRE1α kinase inhibiting RNase attenuator [34], which interferes with the recruitment of TRAF2 [63] and impairs the activation of downstream AP-1 and NF-κB. In view of these, we speculate that the synergies between KIRA6 and FK506 lie in their cooperative regulation of inflammatory signaling pathways, and the expression of NF-κB p65, c-JUN (AP-1), and NAFT-c2 by different preparation-treated SPLCs were determined. Results ascertained that FK506@lipoN did limit the expression of NFAT c-2, with NF-κB p65 downregulated at the same time. Meanwhile, KIRA6@lipoT inhibited NF-κB p65 and JUN (AP-1). When KIRA6@lipoT was used in combination with FK506@lipoN, all three TFs were significantly inhibited (Fig. 7A–D). And Western Blot data (Fig. 7E) further confirmed our conjecture that the synergistic immunosuppressive effect of IRE1α inactivation and calcineurin inhibition lied in a cross-talk between inflammatory TFs and UPR (Fig. 7F).

5. Discussion

A successful organ transplantation depends on: 1. minimized MHC mismatch between donor and recipient; 2. inhibited activation of host immunity; and 3. limited development of host immune memory. High MHC matching is usually too demanding for allogeneic transplantation that has higher accessibility and feasibility. Therefore, it's generally compensated by suppressing the overall immunity of the recipient. Current therapeutic regimen for allogeneic graft mainly relies on limiting the activation of effector lymphocytes, lacking a regulation over immunomemory. However, memory lymphocyte are one of the first to infiltrate the graft [64], with lower activation threshold, less dependence on costimulatory signals, higher resistant to regulatory T cells (Treg), and less sensitivity to traditional immunosuppressants [65,66]. And the generation of lymphocyte alloreactive memory, T-cell memory in particular, may lead to a chronic rejection that impedes the long-term survival of transplanted organs and limits secondary transplantation [8, 50,67]. So far, only a few strategies involving memory regulation in

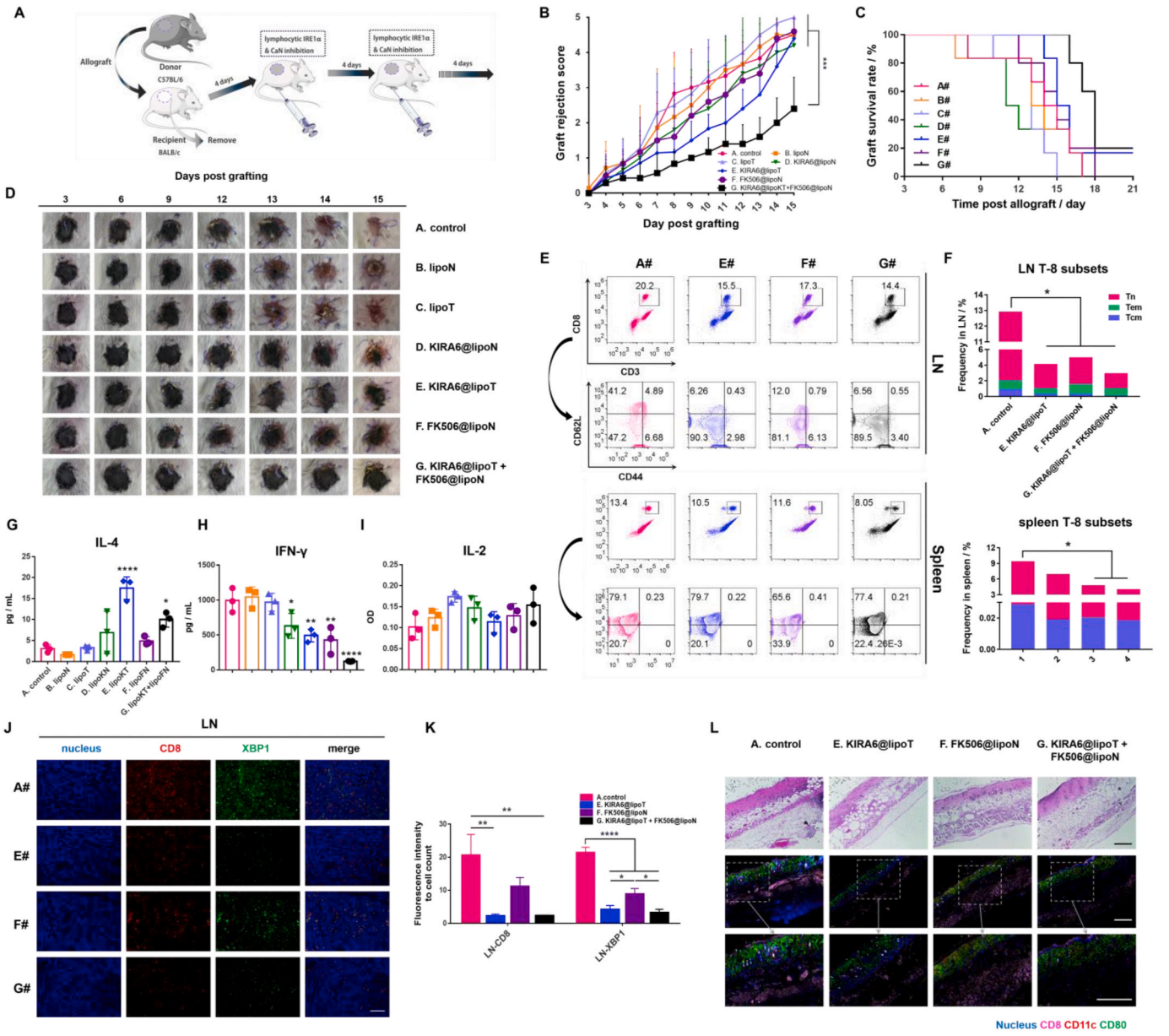

Fig. 6. Anti-rejection efficacy of IRE1α inhibition in murine full-thickness trunk skin allograft. (A) Schematic diagram of the experimental protocol. (B-D) Graft rejection score (B), graft survival rate (C), and representative pictures of grafted skin patch (D) by host mice in different groups, n = 7. (E-F) Representative flow cytometric pictures (E) and summary plot (F) of data showing the frequency of T-8, naïve T-8, effector memory T-8, and central memory T-8 in LN and spleen 7 days post graft, n = 4. (G-I) Determination of IL-4 (G), IFN-γ (H) and IL-2 (I) in serum 7 days post graft using cytokine kits, n = 3. (J-K) Representative immunofluorescence images (J) of axillary LN from each group (blue-nucleus, red-CD8, green-XBP1). Images were analyzed to semiquantitate the fluorescence intensity of CD8 and XBP-1 to cell count (K), n = 3. Scale bar, 200 μm. (L) Representative H&E and immunofluorescence pictures of grafted skin from each group (blue-nucleus, pink-CD8, red-CD11c, green-CD80). Scale bar, 100 μm. All error bars were expressed as mean ± SD. *p < 0.05, **p < 0.01, ***p < 0.001 and ****p < 0.0001. (For interpretation of the references to colour in this figure legend, the reader is referred to the Web version of this article.)

organ transplantation have been proposed and applied, including:

1. Blocking memory T cells from entering the graft. For example, FTY720, a sphingosine-1-phosphate receptor agonist, is used to prevent lymphocytes from migrating to thymus and peripheral lymphoid tissues, which isolates donor-specific memory $CD4^+$ T cells in lymph nodes and prevents their infiltration into the graft, alleviating the rejection of mouse heart transplantation [68]. In addition, inhibiting adhesion molecules, such as leukocyte integrin LFA-1 and VLA4, to prevent memory cells from penetrating into the graft also works [69,70].
2. Inhibiting the proliferation of memory T-lymphocytes. The activation of donor-specific memory T-8 can be blocked by NF-κB inhibitor Deoxyguanidine (DSG), which prolongs the survival of murine allografted skin when used in combination with costimulatory blockade [71].
3. Inducing the depletion of memory T cells [72]. ABT-737, a small molecule inhibitor of Bcl-2/Bcl-XL, was used to induce the apoptosis of alloreactive memory T cells, thus limiting murine skin graft rejection [73].

Unfolded protein response has long been recognized as a principal countermeasure to alleviate endoplasmic reticulum stress, which is currently specified with full potential in regulating lymphocytic immunity for a higher graft survival. Moreover, our strategy of inhibiting lymphocytic IRE1α to induce an overall immunosuppression not only

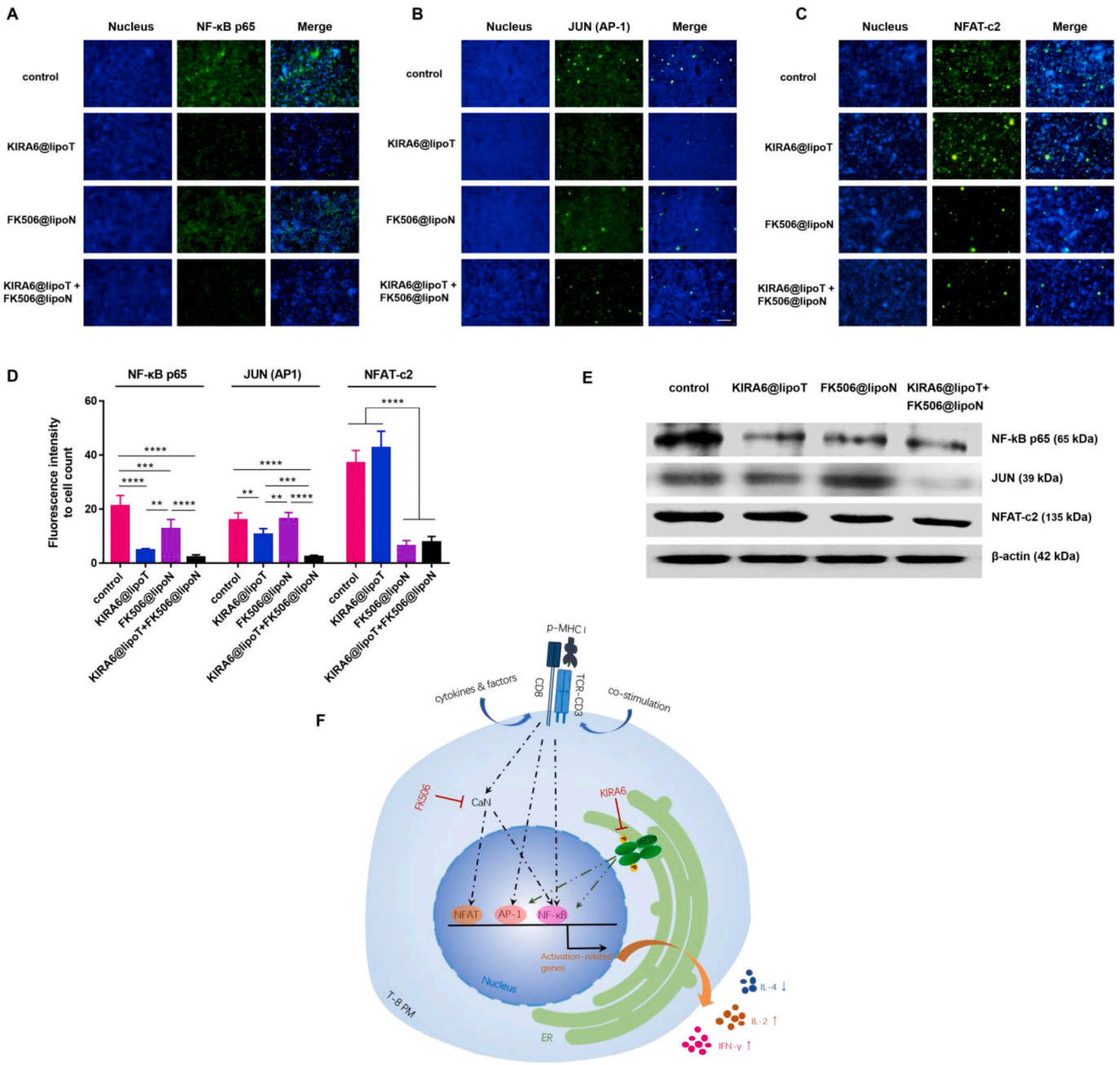

Fig. 7. Synergistic regulation of inflammatory transcription factors by IRE1α and FK506. (A-D) SPLCs were isolated and treated with PRMI 1640, FK506@lipoN (5 nM), KIRA6@lipoT (1.5 μM), or FK506@lipoN (5 nM) plus KIRA6@lipoT (1.5 μM) for 24 h, followed by immunofluorescence staining (green) of NF-κB p65 (A), NFAT-c2 (B), or JUN (C). Nuclei were counterstained with Hoechst 33342 (blue). Scale bar, 100 μm. Quantitative analysis of fluorescent positive cells was shown in (D). n = 4–6. Data are expressed as mean ± SD. *p < 0.05, **p < 0.01, ***p < 0.001 and ****p < 0.0001. (E) Whole-cell extracts of treated cells were collected and analyzed by immunoblotting with NFAT-c2, JUN or NF-κB p65 antibodies, β-actin is used as loading control. (F) Possible intracellular molecular details directing the synergy of IRE1α inactivation and calcineurin inhibition. PM: plasmic membrane, ER: endoplasmic reticulum, CaN: calcineurin inhibitor, FK506: tacrolimus, KIRA6: IRE1α kinase inhibiting RNase attenuator, NFAT: nuclear factor of activated T cells, AP-1: activator protein-1, NF-κB: nuclear factor kappa light chain enhancer of activated B cells. (For interpretation of the references to colour in this figure legend, the reader is referred to the Web version of this article.)

limits the activation of lymphocytes, but abrogates the commitment of immune memory (Figs. 3 and 4), displaying desirable anti-rejection effect in murine full-thickness trunk skin allograft (Fig. 6), which may guide the future treatment of diseases and disorders derived from hyperimmunity, including transplant rejection, inflammatory diseases, autoimmune diseases, type I diabetes mellitus, and type IV hypersensitivity [45–47].

Credit author statement

Yingying Shi: Conceptualization, Methodology, Project administration, Data curation, Writing - original draft, and Writing - review & editing. Yichao Lu: Conceptualization, Methodology, and Data curation. Chunqi Zhu, Zhenyu Luo and Xiang Li: Investigation, Project administration, and Writing - review & editing. Yu Liu, Mengshi Jiang and Xu Liu: Project administration and Data curation. Lihua Luo: Funding acquisition and Writing - review & editing. Yongzhong Du: Supervision and Writing - review & editing. Jian You: Conceptualization,

Methodology, Supervision, Data curation, Writing - review & editing and Funding acquisition.

Funders

National Key R&D Program of China (No. 2017YFE0102200); National Nature Science Foundation of China (81573365, 82003667); Basic Public Welfare Research Project of Zhejiang Province, China (LGF18H300004); China Postdoctoral Science Foundation (2019TQ0283, 2020M671772).

Data availability

The raw/processed data required to reproduce these findings can be shared by the authors upon request.

Declaration of competing interest

The authors declare that they have no known competing financial interests or personal relationships that could have appeared to influence the work reported in this paper.

Acknowledgements

This work was supported by the National Key R&D Program of China (No. 2017YFE0102200), National Natural Science Foundation of China (81573365, 82003667), Basic Public Welfare Research Project of Zhejiang Province, China (LGF18H300004), and China Postdoctoral Science Foundation (2019TQ0283, 2020M671772).

Appendix A. Supplementary data

Supplementary data to this article can be found online at https://doi.org/10.1016/j.biomaterials.2021.120757.

References

[1] J.L. Platt, New directions for organ transplantation, Nature 392 (6679 Suppl) (1998) 11.

[2] M. Abecassis, S.T. Bartlett, A.J. Collins, C.L. Davis, F.L. Delmonico, J.J. Friedewald, R. Hays, A. Howard, E. Jones, A.B. Leichtman, R.M. Merion, R.A. Metzger, F. Pradel, E.J. Schweitzer, R.L. Velez, R.S. Gaston, Kidney transplantation as primary therapy for end-stage renal disease: a national kidney foundation/kidney disease outcomes quality initiative (NKF/KDOQITM) conference, Clin. J. Am. Soc. Nephrol. 3 (2) (2008) 471–480.

[3] F.K. Chiou, S.V. Beath, G.M. Wilkie, M.A. Vickers, B. Morland, G.L. Gupte, Cytotoxic T-lymphocyte therapy for post-transplant lymphoproliferative disorder after solid organ transplantation in children, Pediatr. Transplant. 22 (2) (2018).

[4] R.L. Crepeau, M.L. Ford, Programmed T cell differentiation: implications for transplantation, Cell. Immunol. 351 (2020) 104099.

[5] J. Marino, J. Paster, G. Benichou, Allorecognition by T lymphocytes and allograft rejection, Front. Immunol. 7 (2016) 582.

[6] S.J. Harper, J.M. Ali, E. Wlodek, M.C. Negus, I.G. Harper, M. Chhabra, M. S. Qureshi, M. Mallik, E. Bolton, J.A. Bradley, G.J. Pettigrew, CD8 T-cell recognition of acquired alloantigen promotes acute allograft rejection, Proc. Natl. Acad. Sci. U. S. A. 112 (41) (2015) 12788–12793.

[7] C.A. Su, S. Iida, T. Abe, R.L. Fairchild, Endogenous memory CD8 T cells directly mediate cardiac allograft rejection, Am. J. Transplant. 14 (3) (2014) 568–579.

[8] K. Lin, S. Chen, G. Chen, Role of memory T cells and perspectives for intervention in organ transplantation, Front. Immunol. 6 (2015) 473.

[9] G. Du, N. Yang, W. Gong, Y. Fang, J. He, N. Zhou, X. Lu, Y. Zhao, CD8(+) effector memory T cells induce acute rejection of allogeneic heart retransplants in mice possibly through activating expression of inflammatory cytokines, Exp. Cell Res. 355 (1) (2017) 1–8.

[10] T.C. Wong, C.M. Lo, J.Y. Fung, Emerging drugs for prevention of T-cell mediated rejection in liver and kidney transplantation, Expet Opin. Emerg. Drugs 22 (2) (2017) 1–14.

[11] R.D. Tepperman E, J. Prodger, et al., Surgical biology for the clinician: vascular effects of immunosuppression, Canadian Journal of Surgery Journal Canadien De Chirurgie 53 (1) (2010) 57–63.

[12] L. Liu, M. Zhao, X. Jin, G. Ney, K.B. Yang, F. Peng, J. Cao, T. Iwawaki, J. Del Valle, X. Chen, Q. Li, Adaptive endoplasmic reticulum stress signalling via IRE1alpha-XBP1 preserves self-renewal of haematopoietic and pre-leukaemic stem cells, Nat. Cell Biol. 21 (3) (2019) 328–337.

[13] H. Dong, N.M. Adams, Y. Xu, J. Cao, D.S.J. Allan, J.R. Carlyle, X. Chen, J.C. Sun, L. H. Glimcher, The IRE1 endoplasmic reticulum stress sensor activates natural killer cell immunity in part by regulating c-Myc, Nat. Immunol. 20 (7) (2019) 865–878.

[14] J.R. Cubillos-Ruiz, P.C. Silberman, M.R. Rutkowski, S. Chopra, A. Perales-Puchalt, M. Song, S. Zhang, S.E. Bettigole, D. Gupta, K. Holcomb, L.H. Ellenson, T. Caputo, A.H. Lee, J.R. Conejo-Garcia, L.H. Glimcher, ER stress sensor XBP1 controls anti-tumor immunity by disrupting dendritic cell homeostasis, Cell 161 (7) (2015) 1527–1538.

[15] Y. Cao, J. Trillo-Tinoco, R.A. Sierra, C. Anadon, W. Dai, E. Mohamed, L. Cen, T. L. Costich, A. Magliocco, D. Marchion, R. Klar, S. Michel, F. Jaschinski, R.R. Reich, S. Mehrotra, J.R. Cubillos-Ruiz, D.H. Munn, J.R. Conejo-Garcia, P.C. Rodriguez, ER stress-induced mediator C/EBP homologous protein thwarts effector T cell activity in tumors through T-bet repression, Nat. Commun. 10 (1) (2019) 1280.

[16] K.E. Hurst, K.A. Lawrence, M.T. Essman, Z.J. Walton, L.R. Leddy, J.E. Thaxton, Endoplasmic reticulum stress contributes to mitochondrial exhaustion of CD8(+) T cells, Cancer Immunol Res 7 (3) (2019) 476–486.

[17] J.A. Best, D.A. Blair, J. Knell, E. Yang, V. Mayya, A. Doedens, M.L. Dustin, A. W. Goldrath, C. Immunological Genome Project, Transcriptional insights into the CD8(+) T cell response to infection and memory T cell formation, Nat. Immunol. 14 (4) (2013) 404–412.

[18] R. Brunsing, S.A. Omori, F. Weber, A. Bicknell, L. Friend, R. Rickert, M. Niwa, B-and T-cell development both involve activity of the unfolded protein response pathway, J. Biol. Chem. 283 (26) (2008) 17954–17961.

[19] J.R. Cubillos-Ruiz, P.C. Silberman, M.R. Rutkowski, S. Chopra, A. Perales-Puchalt, M. Song, S. Zhang, S.E. Bettigole, D. Gupta, K. Holcomb, ER stress sensor XBP1 controls anti-tumor immunity by disrupting dendritic cell homeostasis, Cell 161 (7) (2015) 1527–1538.

[20] Y.J. Jeon, S. Khelifa, B. Ratnikov, D.A. Scott, Y. Feng, F. Parisi, C. Ruller, E. Lau, H. Kim, L.M. Brill, T. Jiang, D.L. Rimm, R.D. Cardiff, G.B. Mills, J.W. Smith, A. L. Osterman, Y. Kluger, Z.A. Ronai, Regulation of glutamine carrier proteins by RNF5 determines breast cancer response to ER stress-inducing chemotherapies, Canc. Cell 27 (3) (2015) 354–369.

[21] X. Yuan, B. Qin, H. Yin, Y. Shi, M. Jiang, L. Luo, Z. Luo, J. Zhang, X. Li, C. Zhu, Y. Du, J. You, Virus-like nonvirus cationic liposome for efficient gene delivery via endoplasmic reticulum pathway, ACS Cent. Sci. 6 (2) (2020) 174–188.

[22] H. Yin, X. Yuan, L. Luo, Y. Lu, B. Qin, J. Zhang, Y. Shi, C. Zhu, J. Yang, X. Li, M. Jiang, Z. Luo, X. Shan, D. Chen, J. You, Appropriate delivery of the CRISPR/Cas9 system through the nonlysosomal route: application for therapeutic gene editing, Adv. Sci. 7 (14) (2020) 1903381.

[23] C.F.L. Chih–Hsien Cheng, Madeline Fryer, Georg J. Furtmüller, Byoungchol Oh, Jonathan D. Powell, Gerald Brandacher, Murine full-thickness skin transplantation, JoVE 119 (2017), e55105.

[24] B.J. Schwoebel F, A. Wendel, J. Hamacher, Quantitative assessment of mouse skin transplant rejection using digital photography, Lab. Anim. 39 (2) (2005) 209–214.

[25] F.O. Bagger, D. Sasivarevic, S.H. Sohi, L.G. Laursen, S. Pundhir, C.K. Sonderby, O. Winther, N. Rapin, B.T. Porse, BloodSpot: a database of gene expression profiles and transcriptional programs for healthy and malignant haematopoiesis, Nucleic Acids Res. 44 (D1) (2016) D917–D924.

[26] M.W. Painter, S. Davis, R.R. Hardy, D. Mathis, C. Benoist, C, Immunological Genome Project, Transcriptomes of the B and T lineages compared by multiplatform microarray profiling, J. Immunol. 186 (5) (2011) 3047–3057.

[27] A.S. Martins, I. Alves, L. Helguero, M.R. Domingues, B.M. Neves, The unfolded protein response in homeostasis and modulation of mammalian immune cells, Int. Rev. Immunol. 35 (6) (2016) 457–476.

[28] T.S. Heng, M.W. Painter, K. Elpek, V. Lukacs-Kornek, N. Mauermann, S.J. Turley, D. Koller, F.S. Kim, A.J. Wagers, N. Asinovski, S. Davis, The immunological genome project networks of gene expression in immune cells, Nat. Immunol. 9 (2008) 1091–1094.

[29] P.H. Krammer, CD95's deadly mission in the immune system, Nature 407 (2000) 789–795.

[30] A.G. Lerner, J.P. Upton, P.V. Praveen, R. Ghosh, Y. Nakagawa, A. Igbaria, S. Shen, V. Nguyen, B.J. Backes, M. Heiman, N. Heintz, P. Greengard, S. Hui, Q. Tang, A. Trusina, S.A. Oakes, F.R. Papa, IRE1alpha induces thioredoxin-interacting protein to activate the NLRP3 inflammasome and promote programmed cell death under irremediable ER stress, Cell Metabol. 16 (2) (2012) 250–264.

[31] M.D. Bright, D.N. Itzhak, C.P. Wardell, G.J. Morgan, F.E. Davies, Cleavage of BLOC1S1 mRNA by IRE1 is sequence specific, temporally separate from XBP1 splicing, and dispensable for cell viability under acute endoplasmic reticulum stress, Mol. Cell Biol. 35 (12) (2015) 2186–2202.

[32] J. Lebeau, J.M. Saunders, V.W.R. Moraes, A. Madhavan, N. Madrazo, M. C. Anthony, R.L. Wiseman, The PERK arm of the unfolded protein response regulates mitochondrial morphology during acute endoplasmic reticulum stress, Cell Rep. 22 (11) (2018) 2827–2836.

[33] M. Mahameed, T. Wilhelm, O. Darawshi, A. Obiedat, W.S. Tommy, C. Chintha, T. Schubert, A. Samali, E. Chevet, L.A. Eriksson, M. Huber, B. Tirosh, The unfolded protein response modulators GSK2606414 and KIRA6 are potent KIT inhibitors, Cell Death Dis. 10 (4) (2019) 300.

[34] R. Ghosh, L. Wang, E.S. Wang, B.G. Perera, A. Igbaria, S. Morita, K. Prado, M. Thamsen, D. Caswell, H. Macias, K.F. Weiberth, M.J. Gliedt, M.V. Alavi, S. B. Hari, A.K. Mitra, B. Bhhatarai, S.C. Schurer, E.L. Snapp, D.B. Gould, M. S. German, B.J. Backes, D.J. Maly, S.A. Oakes, F.R. Papa, Allosteric inhibition of the IRE1alpha RNase preserves cell viability and function during endoplasmic reticulum stress, Cell 158 (3) (2014) 534–548.

[35] M.H. Spitzer, Y. Carmi, N.E. Reticker-Flynn, S.S. Kwek, D. Madhireddy, M. M. Martins, P.F. Gherardini, T.R. Prestwood, J. Chabon, S.C. Bendall, L. Fong, G.

P. Nolan, E.G. Engleman, Systemic immunity is required for effective cancer immunotherapy, Cell 168 (3) (2017) 487–502 e15.
[36] A.L. Ackerman, C. Kyritsis, R. Tampe, P. Cresswell, Access of soluble antigens to the endoplasmic reticulum can explain cross-presentation by dendritic cells, Nat. Immunol. 6 (1) (2005) 107–113.
[37] J. Imai, H. Hasegawa, M. Maruya, S. Koyasu, I. Yahara, Exogenous antigens are processed through the endoplasmic reticulum-associated degradation (ERAD) in cross-presentation by dendritic cells, Int. Immunol. 17 (1) (2005) 45–53.
[38] Y. Shi, C. Zhu, Y. Liu, Y. Lu, X. Li, B. Qin, Z. Luo, L. Luo, M. Jiang, J. Zhang, G. Guan, C. Zheng, J. You, A vaccination with boosted cross presentation by ER-targeted antigen delivery for anti-tumor immunotherapy, Adv Healthc Mater (2021), e2001934.
[39] W.Y. Xie, X.D. Zhou, Q. Li, L.X. Chen, D.H. Ran, Acid-induced autophagy protects human lung cancer cells from apoptosis by activating ER stress, Exp. Cell Res. 339 (2) (2015) 270–279.
[40] S. Janssens, B. Pulendran, B.N. Lambrecht, Emerging functions of the unfolded protein response in immunity, Nat. Immunol. 15 (10) (2014) 910–919.
[41] M.J. Topper, M. Vaz, K.A. Marrone, J.R. Brahmer, S.B. Baylin, The emerging role of epigenetic therapeutics in immuno-oncology, Nat. Rev. Clin. Oncol. 17 (9) (2019).
[42] K. Araki, M. Morita, A.G. Bederman, B.T. Konieczny, H.T. Kissick, N. Sonenberg, R. Ahmed, Translation is actively regulated during the differentiation of CD8(+) effector T cells, Nat. Immunol. 18 (9) (2017) 1046–1057.
[43] S.M. Kaech, R. Ahmed, Memory CD8+ T cell differentiation: initial antigen encounter triggers a developmental program in naive cells, Nat. Immunol. 2 (5) (2001) 415–422.
[44] E.J.W.a.R. Ahmed, Memory CD8 T-cell differentiation during viral infection, J. Virol. 78 (11) (2004) 5535–5545.
[45] P. Serra, P. Santamaria, Antigen-specific therapeutic approaches for autoimmunity, Nat. Biotechnol. 37 (3) (2019) 238–251.
[46] X. Luo, S.D. Miller, L.D. Shea, Immune tolerance for autoimmune disease and cell transplantation, Annu. Rev. Biomed. Eng. 18 (2016) 181–205.
[47] C. Shimokawa, T. Kato, T. Takeuchi, N. Ohshima, T. Furuki, Y. Ohtsu, K. Suzue, T. Imai, S. Obi, A. Olia, T. Izumi, M. Sakurai, H. Arakawa, H. Ohno, H. Hisaeda, CD8(+) regulatory T cells are critical in prevention of autoimmune-mediated diabetes, Nat. Commun. 11 (1) (2020) 1922.
[48] L. Luo, C. Li, W. Wu, J. Lu, Y. Zhou, J. Shan, S. Li, D. Long, Y. Guo, Y. Li, L. Feng, Functional analysis of alloreactive memory CD4+ T cells derived from skin transplantation recipient and naive CD4+ T cells derived from untreated mice, J. Surg. Res. 176 (2) (2012) 649–656.
[49] G. Benichou, Y. Yamada, S.H. Yun, C. Lin, M. Fray, G. Tocco, Immune recognition and rejection of allogeneic skin grafts, Immunotherapy 3 (6) (2011) 757–770.
[50] N.J. Felix, P.M. Allen, Specificity of T-cell alloreactivity, Nat. Rev. Immunol. 7 (12) (2007) 942–953.
[51] D.M. Supp, S.T. Boyce, Engineered skin substitutes: practices and potentials, Clin. Dermatol. 23 (4) (2005) 403–412.
[52] S.T. Boyce, A.L. Lalley, Tissue engineering of skin and regenerative medicine for wound care, Burns Trauma 6 (2018) 4.
[53] C.R. Gardner, The pharmacology of immunosuppressant drugs in skin transplant rejection in mice and other rodents, Gen. Pharmacol. Vasc. Syst. 26 (2) (1995) 245–271.
[54] M. Tong, Y. Jiang, FK506-binding proteins and their diverse functions, Curr. Mol. Pharmacol. 9 (1) (2015) 48–65.
[55] A.O. Shigeki Tamura, Rinta Ibuki, Gordon L. Amidon, Shinji Yamashita, Tacrolimus is a class II low-solubility high-permeability drug: the effect of P-glycoprotein efflux on regional permeability of tacrolimus in rats, J. Pharmaceut. Sci. 91 (3) (2002) 719–729.
[56] Z. Solhjou, H. Athar, Q. Xu, R. Abdi, Emerging therapies targeting intra-organ inflammation in transplantation, Am. J. Transplant. 15 (2) (2015) 305–311.
[57] P.F. Halloran, C. Kreepala, G. Einecke, A. Loupy, J. Sellarés, Therapeutic Approaches to Organ Transplantation, John Wiley & Sons, 2015. Ltd.
[58] A. Vandewalle, E. Tourneur, M. Bens, C. Chassin, C. Werts, Calcineurin/NFAT signaling and innate host defence: a role for NOD1-mediated phagocytic functions, Cell Commun. Signal. 12 (2014) 8.
[59] J. Grootjans, A. Kaser, R.J. Kaufman, R.S. Blumberg, The unfolded protein response in immunity and inflammation, Nat. Rev. Immunol. 16 (8) (2016) 469–484.
[60] X.W. Fumihiko Urano, Anne Bertolotti, Yuhong Zhang, Peter Chung, Heather P. Harding, David Ron, Coupling of stress in the ER to activation of JNK protein kinases by transmembrane protein kinase IRE1, Science 287 (5453) (2000) 664–666.
[61] C. Hetz, F. Martinon, D. Rodriguez, L.H. Glimcher, The unfolded protein response: integrating stress signals through the stress sensor IRE1α, Physiol. Rev. 91 (2011) 1219–1243.
[62] M. Kaneko, Y. Niinuma, Y. Nomura, Activation signal of nuclear factor-kappa B in response to endoplasmic reticulum stress is transduced via IRE1 and tumor necrosis factor receptor-associated factor 2, Biol. Pharm. Bull. 26 (7) (2003) 931–935.
[63] A.M. Keestra-Gounder, M.X. Byndloss, N. Seyffert, B.M. Young, A. Chavez-Arroyo, A.Y. Tsai, S.A. Cevallos, M.G. Winter, O.H. Pham, C.R. Tiffany, M.F. de Jong, T. Kerrinnes, R. Ravindran, P.A. Luciw, S.J. McSorley, A.J. Baumler, R.M. Tsolis, NOD1 and NOD2 signalling links ER stress with inflammation, Nature 532 (7599) (2016) 394–397.
[64] Z.D. Geetha Chalasani, Bogumila T. Konieczny, Fady K. Baddoura, Fadi G. Lakkis, Recall and propagation of allospecific memory T cells independent of secondary lymphoid organs, Proc. Natl. Acad. Sci. Unit. States Am. 99 (9) (2002) 6175–6180.
[65] J.Y.e. al, Allograft rejection mediated by memory T cells is resistant to regulation, Proc. Natl. Acad. Sci. Unit. States Am. 104 (50) (2007) 19954–19959.
[66] C.A. Su, R.L. Fairchild, Memory T cells in transplantation, Curr Transplant Rep 1 (3) (2014) 137–146.
[67] A. Valujskikh, The challenge of inhibiting alloreactive T-cell memory, Am. J. Transplant. 6 (4) (2006) 647–651.
[68] Q. Zhang, Y. Chen, R.L. Fairchild, P.S. Heeger, A. Valujskikh, Lymphoid sequestration of alloreactive memory CD4 T cells promotes cardiac allograft survival, J. Immunol. 176 (2) (2006) 770–777.
[69] J. Xia, J. Chen, W. Shao, T. Lan, Y. Wang, B. Xie, H. Thorlacius, F. Tian, R. Huang, Z. Qi, Suppressing memory T cell activation induces islet allograft tolerance in alloantigen-primed mice, Transpl. Int. 23 (11) (2010) 1154–1163.
[70] M. Carvalho-Gaspar, N.D. Jones, S. Luo, L. Martin, M.O. Brook, K.J. Wood, Location and time-dependent control of rejection by regulatory T cells culminates in a failure to generate memory T cells, J. Immunol. 180 (10) (2008) 6640–6648.
[71] L.L. Molinero, P. Zhou, Y. Wang, H. Harlin, B. Kee, C. Abraham, M.L. Alegre, Epidermal Langerhans cells promote skin allograft rejection in mice with NF-kappa B-impaired T cells, Am. J. Transplant. 8 (1) (2008) 21–31.
[72] R. Valdez-Ortiz, O. Bestard, I. Llaudo, M. Franquesa, G. Cerezo, J. Torras, I. Herrero-Fresneda, R. Correa-Rotter, J.M. Grinyo, Induction of suppressive allogeneic regulatory T cells via rabbit antithymocyte polyclonal globulin during homeostatic proliferation in rat kidney transplantation, Transpl. Int. 28 (1) (2015) 108–119.
[73] P.E. Cippa, S.S. Gabriel, A.K. Kraus, J. Chen, T. Wekerle, A. Guimezanes, R. P. Wuthrich, T. Fehr, Bcl-2 inhibition to overcome memory cell barriers in transplantation, Am. J. Transplant. 14 (2) (2014) 333–342.